Astrophys Space Sci (2019) 364:154
https://doi.org/10.1007/s10509-019-3646-5

ORIGINAL ARTICLE

Space weather and hurricanes Irma, Jose and Katia

Yaroslav Vyklyuk[1,2] · Milan M. Radovanović[3,4] · Boško Milovanović[3] · Milan Milenković[3] · Marko Petrović[3,4] · Dejan Doljak[3] · Slavica Malinović Milićević[5] · Natalia Vuković[6] · Aleksandra Vujko[7] · Nataliia Matsiuk[8] · Saumitra Mukherjee[9]

Received: 10 January 2019 / Accepted: 10 September 2019

Abstract This research is devoted to the determination of the causal relationship between the flow of particles that are coming from the Sun and the hurricanes Irma, Jose, and Katia. To accomplish this, the lag correlation analysis was performed. High correlation coefficients confirmed a preliminary conclusion about the relationship between solar activities and the hurricane phenomenon, which allows further research. Five parameters i.e. characteristics of solar activity (10.7 cm solar radio flux (F10.7), the flows of protons and electrons with maximum energy, speed and density of solar wind particles) were chosen as model input, while the wind speed and air pressure of Irma, Jose, and Katia hurricanes were used as model output. Input data were sampled to a six hours interval in order to adapt the time interval to the observed data about hurricanes, in the period between September 28 and December 21, 2017. As a result of the preliminary analysis, using 12,274,264 linear models by parallel calculations, six of them were chosen as best. The identified lags were the basis for refinement of models with the artificial neural networks. Multilayer perceptrons with back propagation and recurrent LSTM have been chosen as commonly used artificial neural networks. Comparison of the accuracy of both linear and artificial neural networks results confirmed the adequacy of these models and made it possible to take into account the dynamics of the solar wind. Sensitivity analysis has shown that F10.7 has the greatest impact on the wind speed of the hurricanes. Despite low sensitivity of pressure to change the parameters of the solar wind, their strong fluctuations can cause a sharp decrease in pressure, and therefore the appearance of hurricanes.

Keywords Charged particles · Atmospheric disturbances · Artificial neural network · Hurricanes

✉ D. Doljak
d.doljak@gi.sanu.ac.rs

1 Institute of Laser and Optoelectronic Intelligent Manufacturing, College of Mechanical and Electrical Engineering, Wenzhou University, Wenzhou 325035, P.R. China

2 Bukovinian University, Darvina str. 2A, Chernivtsi 58000, Ukraine

3 Geographical Institute "Jovan Cvijić", Serbian Academy of Sciences and Arts, Djure Jakšića 9, 11000 Belgrade, Serbia

4 Institute of Sports, Tourism and Service, South Ural State University, Soni Krivoi str., 60, Chelyabinsk 454080, Russia

5 University Center for Meteorology and Environmental Modelling, University of Novi Sad, Dr Zorana Djindjića 1, 21000 Novi Sad, Serbia

6 Graduate School of Economics and Management, The Ural Federal University Named after the First President of Russia B.N. Yeltsin, 19 Mira St., Yekaterinburg 620002, Russia

7 Novi Sad Business School, Vladimira Perića Valtera 4, 21000 Novi Sad, Serbia

8 Yuriy Fedkovych Chernivtsi National University, 2 Kotsjubynskyi Str. Chernivtsi 58012, Ukraine

9 School of Environmental Sciences, Jawaharlal Nehru University, New Delhi 110067, India

1 Introduction

The solar proton anomaly and its impact on the Earth has improved the understanding of environment changes induced by the Sun (Mukherjee 2013). Sudden changes in the terrestrial temperature have some bearing with the proton flux anomaly (Mukherjee 2015). At the end of August and beginning of September 2017, the instruments on the Advanced Composition Explorer (ACE) satellite measured the unusually strong flow of high-energy particles. Then, in the geoeffective position, there was a coronary hole rising from the northern polar region of the Sun across its equator, as

Published online: 16 September 2019

well as the energy regions 12671 and 12672 (SolarMonitor.org 2017). The satellite is otherwise located in the Lagrange point so that in real time it measures the parameters of the solar wind (SW). During the first half of September, more than a dozen M-class flashes, an X-9 level flare and an associated moderate solar particle event (SPE) appeared in the geo-effective position. On September 7 and 8, 2017, the early arrival of the coronal mass ejection (CME) associated with the X-9 flare produced severe geomagnetic storming. Simultaneously with these processes in the Sun, in the atmosphere over the Atlantic, some disturbances developed into the hurricanes Irma, Jose, and Katia, where Irma was one of the most devastating hurricanes ever recorded (Japan Aerospace Exploration Agency Earth Observation Research Center 2017).

It can be said that there are numerous concerns about both the occurrence of cyclone disorders and their behavior in time and space (Frank and Young 2007). The analysis of surface pressure variations after SPEs and Forbush decreases for the Eurasian region has shown significant variations of this atmospheric pressure during at least the first five days after the events. These variations differ alongside latitude and longitude. There are cells of increased and reduced surface pressure (Morozova et al. 2002; Mihajlović 2017).

Hodges et al. (2014), Radovanović (2018) bring a list of references that verify the idea of the causal-consequence link of processes in the Sun with hurricanes, dating back to the 19th century.

A spatially heterogeneous response in hurricane intensity and frequency is observed in response to changes in solar activity (Elsner et al. 2008). Hodges and Elsner (2012) argued that regional hurricane frequency from 1851 to 2010 indicates fewer hurricanes across the Caribbean and along the eastern seaboard of the USA when sunspots are numerous. In contrast, fewer hurricanes are observed in the central and eastern North Atlantic when sunspots are few. A significant positive correlation between the averaged *Kp* index of global geomagnetic activity and hurricane intensity as measured by maximum sustained wind speed is identified for baroclinically-initiated hurricanes (Elsner and Kavlakov 2001).

Solar radiation has an important influence on the entire Earth's atmosphere (Bajčetić et al. 2015; Todorović Drakul et al. 2016). It has been long noted that the solar-associated climate anomalies in the troposphere are largely of stratospheric origin (Haigh 1996). It is observed that significant weather events, particularly if caused by low pressure systems, tend to follow arrivals of the high-speed solar wind (Prikryl et al. 2017). Previously published statistical evidence that explosive extratropical cyclones in the northern hemisphere tend to occur within a few days after arrivals of high-speed solar wind streams from coronal holes (Prikryl et al. 2009a,b, 2016) is corroborated for the southern hemisphere.

It has been found that solar cosmic ray bursts result in an increase in the duration of elementary synoptic processes in the Atlantic–European sector of the Northern Hemisphere. It has been assumed that the observed variations in the elementary synoptic processes duration are caused by the effect of short period cosmic ray variations on the intensity of cyclonic processes at middle and high latitudes (Veretenenko and Thejll 2004; Artamonova and Veretenenko 2013; Veretenenko 2017).

Applying wavelet spectral analysis to the hurricane time series, Mendoza and Pazos (2009) found periodicities that coincide with the main sunspot and magnetic solar cycles. In the Atlantic Ocean, there are peaks near 11 and 22 years. Their results indicate that the highest significant correlations are found between the Atlantic and Pacific hurricanes and the *Dst* index. Most importantly, both oceans present the highest hurricane – *Dst* correlations during the ascending part of odd solar cycles and the descending phase of even solar cycles.

First, we could say, surprisingly successful forecasts were published by P. Corbyn for 6–11 months in advance. The methods he used were related solely to variations in the behavior of the Sun, its magnetic field, coronal eruptions, and fluctuating character of the solar wind. The result was that in the period from October 1995 to September 1997, four out of five strong storms were accurately forecasted. The fifth one had an error of 48 hours (Wheeler 2001).

Vyklyuk et al. (2017a) have tried, using the ANFIS model, to determine if there is a mathematical connection between the flow of high energy particles from the Sun and the number of hurricanes. For the period 1999–2013 (daily values from May to October), with a phase shift of 0–3 days, it was found that the models can explain at best 22%–26% of the potential connectivity. In another attempt, Vyklyuk et al. (2017b), for the same period, used better computer equipment and extended the phase shift from 0–10 days, which obtained better results (up to 39%). The authors conclude that these results cannot be ignored and that additional efforts are needed to explain the cause-and-effect relationships. In that sense, we considered that it would also be necessary to examine the causal relationship between the flow of particles from the Sun and the formation of hurricanes Irma, Katia, and Jose.

Unlike the mentioned studies where the period from 1999–2013 was processed, in this paper, the focus is on three specific cases, i.e. establish a possible cause-consequential connection with certain examples, where the event times overlap and refer to the interval up to 16 days. Considering that the implementation of the appropriate procedures has concluded that on a long-term basis a certain connection exists, it was challenging to apply the same methods, in order to investigate which results can be obtained for a period of few weeks.

Table 1 The main characteristics of the investigated hurricanes

	Irma	Jose	Katia
The beginning	30 Aug. 2017 at 12:00 UTC	5 Sep. 2017 at 12:00 UTC	5 Sep. 2017 at 18:00 UTC
The end	12 Sep. 2017 at 00:00 UTC	21 Sep. 2017 at 18:00 UTC	9 Sep. 2017 at 20:00 UTC
Date of maximum wind speed	6 Sep. 2017 at 6:00 UTC	9 Sep. 2017 at 11:00 UTC	8 Sep. 2017 at 18:00 UTC
Duration	13 days	16 days	4 days
Sampling	6 hr	6 hr	6 hr
Number of observations	52	66	15

2 Input data analysis

The Unisys (2017) was the source of data on hurricanes Irma, Jose, and Katia. The data included maximum sustained winds in knots, and central pressure in millibar (mb) for periods of 6 hours (0–6 hr, 6–12 hr, 12–18 hr, and 18–24 hr). The 5-minute data on solar particle and electron fluxes (source: GOES-15) were provided by the Space Weather Prediction Center (2017a). The particles are protons (P) at >1 MeV, >5 MeV, >10 MeV, >30 MeV, >50 MeV, and >100 MeV. The data on electrons (E) included >0.8 MeV and >2.0 MeV. The source of daily solar F10.7 cm (2 800 MHz) was the Space Weather Prediction Center (2017b). The data on proton speed (km/s) and proton density (protons per cubic centimetre) were obtained from the data archive of the SOHO CELIAS Proton Monitor (2017).

The task was to find functional dependencies between the solar wind (SW) parameters and the main characteristics of hurricanes. The main characteristics of the dataset are shown in Table 1. The main investigated criteria (like output) were the speed of wind and pressure. As one can see from Table 1, the data for each hurricane were updated every 6 hours.

Each record represents an averaged metric for the specified sampling interval. The dynamics of the mentioned above characteristics are shown in Fig. 1a and 1b.

As can be seen in Fig. 1a, each hurricane has a pronounced peak (black arrows) in the wind speed graph. Each of these peaks, accordingly to the Bernoulli's law, corresponded to the minimum pressure at the hurricane epicenter. It is also clear that these hurricanes reached their maximum wind speed with a difference of 1–3 days. So we can assume that they are caused by the same factors. As was shown in the paper (Vyklyuk et al. 2017a), the parameters of solar activity can be used as approximations of these factors.

3 Preliminary processing of input data

The characteristics of SW which were tested in the work (like input parameters) include flows of protons and electrons of different energies, a complex indicator of solar wind – 10.7, speed and density of the particles of SW. The main characteristics of the set of input data are given in Table 2.

As one can see from Table 2, the range of input parameters is greater than that of the output ones. It allows us to take into account lag dependencies without reducing the number of the time series. It should be noted that the sampling of measurement of values in all cases except for F10.7 is greater than the studied output values (see Table 1). In further research the sampling of all input data was reduced to six hours by averaging:

$$\overline{In}(t_i) = \sum_{j=i-b}^{i-1} In(t_j)/b, \quad (1)$$

where In is time series of the input parameter, b is the number of averaged data, and j is moment (index of record) of time in the time series.

The averaging was made taking into account that the value at a given moment $In(t_j)$ is averaged over the entire previous period between measurements, not including measurements at a given time. In the case of time series of electrons and protons, the value of blocks of averaged data was $b = 72$. Respectively for speed and wind density: $b = 6$. This averaging helped to eliminate the problem of missing data, which was sometimes observed in time series.

In the case of the F10.7 time series, whose sampling is greater than the output fields, the data were interpolated with a sampling of 6 hours. The cubic spline interpolation using Hermite polynomials (PCHIP) was used (Fritsch and Carlson 1980). Interpolation results are presented in Fig. 2.

As can be seen from Fig. 2, the graph has no oscillations but has pronounced extrema at points 4 and 7 September 2017. This is ahead of the peaks of studied hurricanes, from two to five days, respectively. So, in order to take into account the influence of these two peaks, in case of finding the relationship between this factor and the output fields, the lag delay can be equal from 8 to 20 six-hour intervals.

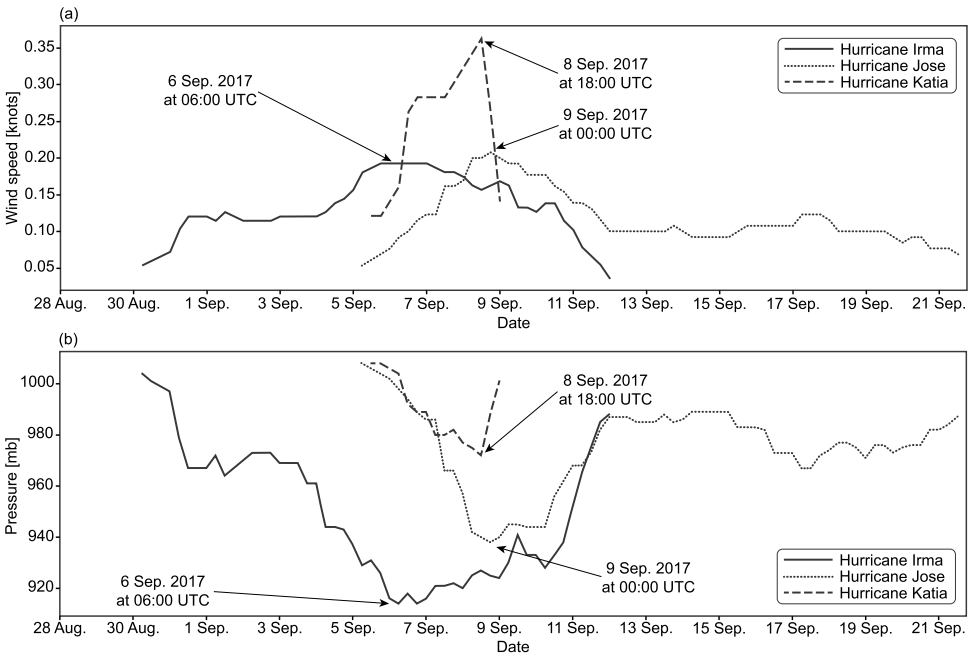

Fig. 1 Wind speed (a) and pressure (b) for hurricanes Irma, Jose and Katia. Black arrows represent dates of the maximum wind speed and minimum air pressure, respectively

Table 2 Characteristics of the SW set

The characteristics of solar activity	Units of measurement	The beginning	The end	Sampling
$P > 1$, $P > 5$, $P > 10$, $P > 30$, $P > 50$, and $P > 100$	Protons (> MeV)/(cm^2·s)	28 Aug. 2017 at 00:00 UTC	22 Sep. 2017 at 00:00 UTC	5 min
$E > 0.8$ and $E > 2.0$	Electrons (> MeV)/(cm^2·s)	28 Aug. 2017 at 00:00 UTC	22 Sep. 2017 at 00:00 UTC	5 min
F10.7		28 Aug. 2017 at 00:00 UTC	21 Sep. 2017 at 00:00 UTC	1 day
Proton speed	km/s	28 Aug. 2017 at 00:00 UTC	22 Sep. 2017 at 00:00 UTC	1 hour
Proton density	Protons/cm^3	28 Aug. 2017 at 00:00 UTC	22 Sep. 2017 at 00:00 UTC	1 hour

4 Correlation analysis

To find the relationship between input factors, a correlation analysis (Cohen et al. 2013) was carried out (see Table 3).

As can be seen from Table 3, there is a strong correlation between the time series of proton flows. The situation is the same for the electron flows. So, the number of input factors can be significantly reduced. In order to select the most appropriate factor, the time series was normalized and depicted on a single graph (Fig. 3a, 3b, and 3c).

As can be seen from Fig. 3a, all normalized factors that describe the flow of protons are characterized by the same dynamics. Namely, all 6 time series have two distinct peaks. The first peak corresponds to the date September 7, 2017, the second to September 11, 2017. Namely, the first came later after the wind speed extreme hurricane Irma and somewhat ahead of the hurricanes Jose and Katia. The second peak appears after all three hurricanes, so it is unlikely that the flow of protons affects the appearance of hurricanes.

As can be seen from Fig. 3b, the behavior of electron fluxes of different energies is quite similar. There are pronounced oscillations on the graphs that are not visually observed in the dynamics of studied characteristics of hurricanes. The behavior of the SW (Fig. 3c) also significantly differs from Fig. 1. That is why there is a low probability of influence of these factors on the wind power and hurricane air pressure.

To confirm or refute these conclusions a lag correlation analysis was conducted, which allowed to find a correlation between the separate time series of input factors displaced for a certain number of rows vertically down (lag) and output factors (Olden and Neff 2001). The lag was investigated in

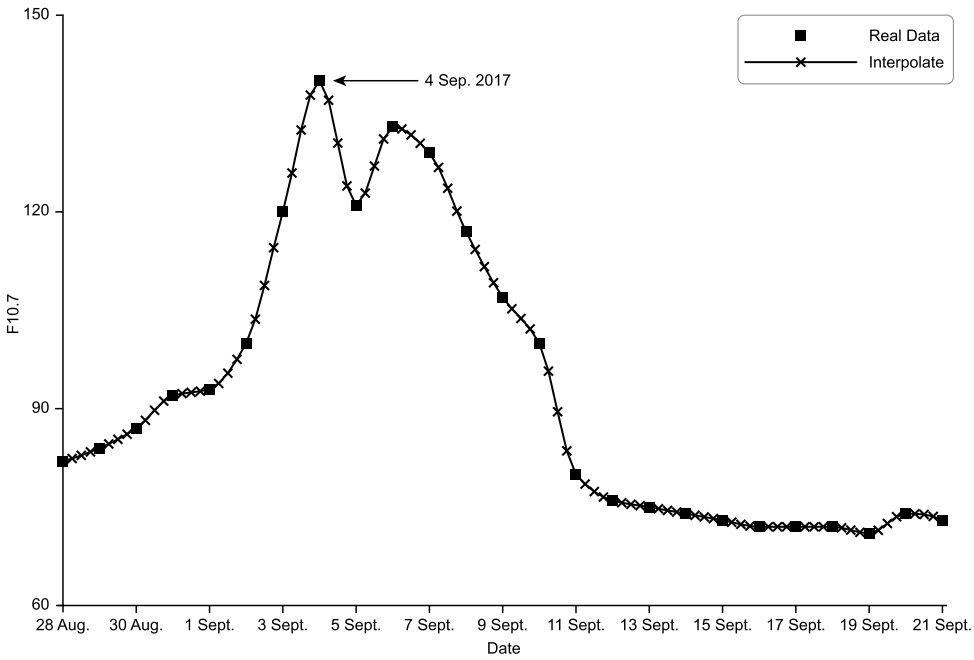

Fig. 2 Interpolation of F10.7 for sampling of 6 hours

Table 3 Correlation analysis of input factors

	P > 1	P > 5	P > 10	P > 30	P > 50	P > 100	E > 0.8	E > 2.0	Speed	Density	F10.7
P > 1	1.00										
P > 5	0.77	1.00									
P > 10	0.66	0.97	1.00								
P > 30	0.56	0.91	0.98	1.00							
P > 50	0.52	0.87	0.95	0.99	1.00						
P > 100	0.45	0.78	0.87	0.94	0.98	1.00					
E > 0.8	−0.19	−0.12	−0.05	0.01	0.03	0.06	1.00				
E > 2.0	−0.20	−0.17	−0.12	−0.09	−0.07	−0.06	0.81	1.00			
Speed	0.26	0.11	0.09	0.07	0.07	0.07	0.13	0.02	1.00		
Density	0.27	0.13	0.09	0.07	0.06	0.04	−0.38	−0.19	0.00	1.00	
F10.7	0.12	−0.04	−0.15	−0.20	−0.19	−0.16	−0.07	−0.22	−0.11	−0.10	1.00

the range from 0 to 20 sampling (5 days). The results of the analysis of the maximum and minimum values of the correlation coefficient depending on the lag are represented in Table 4.

Calculations show that errors consist only 8–10% of correlation coefficients absolute values. As can be seen from Table 4, the highest correlation coefficient R is observed for the factor F10.7 for the Irma hurricane: $R_{wind\ speed} = 0.86$ ($lag = 6$), $R_{pr} = -0.91$ – pressure (lag = 9). Then Katia ($lag = 17$) $R_{wind\ speed} = 0.84$, and $R_{pr} = -0.91$. The hurricane Jose has the smallest correlation coefficient (lag = 18) $R_{wind\ speed} = 0.72$ and $R_{pr} = -0.47$. Negative values of correlation coefficients for pressure time series prove an inverse relationship between the input factor and the output one. This confirms the preliminary conclusions about the relationship between this factor and hurricane parameters.

As results from Table 4 show, that taking into account lag shift of time series, correlation coefficients of other factors essentially increased, including the electron flux and characteristics of the SW. The flow of protons has a high correlation coefficient only for the Katia hurricane. This may be explained due to a small number of observations for this hurricane (Table 1). To establish the functional dependence of this, further analysis is required. In the absence of a physical hypothesis and the availability only time series, the best approximation is the Data Mining approach.

In addition, the distribution of lags with maximum (minimum) correlation coefficients is significant for different input variables. Thus, high correlation coefficients and the un-

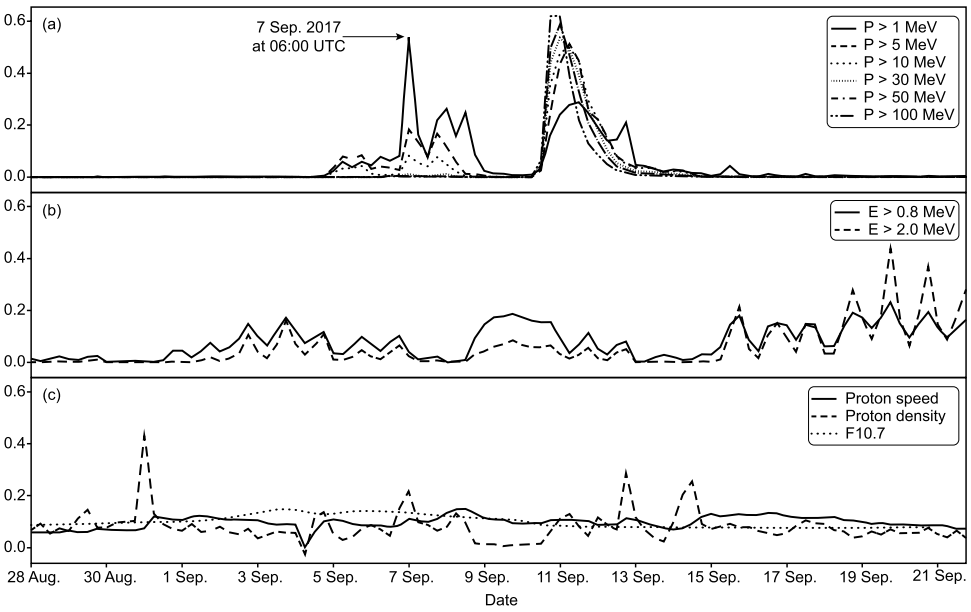

Fig. 3 Normalized input parameters of proton flows (a), electron flows (b), speed, density, and F(c)

Table 4 Consolidated correlation lag analysis of input factors

	P > 1	P > 5	P > 10	P > 30	P > 50	P > 100	E > 0.8	E > 2.0	Speed	Density	F10.7
Wind speed of the Irma hurricane											
Max	0.21	0.37	0.33	0.20	0.20	0.18	0.73	0.54	0.39	0.07	0.86
Lag	6	6	7	7	7	9	14	13	20	7	6
Pressure of the Irma hurricane											
Min	−0.38	−0.46	−0.43	−0.33	−0.33	−0.22	−0.81	−0.61	−0.51	0.03	−0.91
Lag	7	6	7	7	7	9	14	14	20	7	9
Wind speed of the Jose hurricane											
Max	0.44	0.13	0.12	0.13	0.14	0.16	0.18	0.21	0.45	0.15	0.72
Lag	7	0	0	0	0	0	20	20	3	12	18
Pressure of the Jose hurricane											
Min	−0.37	−0.02	−0.02	−0.07	−0.09	−0.11	−0.33	−0.25	−0.53	−0.24	−0.47
Lag	7	10	0	0	0	0	0	20	4	12	19
Wind speed of the Katia hurricane											
Max	0.55	0.57	0.65	0.68	0.62	0.74	0.68	0.61	0.66	0.51	0.84
Lag	0	9	11	2	12	11	19	19	0	1	17
Pressure of the Katia hurricane											
Min	−0.58	−0.70	−0.68	−0.76	−0.65	−0.77	−0.76	−0.68	−0.71	−0.53	−0.91
Lag	1	9	11	2	2	11	19	19	0	1	17

resolved issue of lags cause further research to find functional relationships between these input and output parameters. Therefore, F10.7, the flows of protons and electrons with maximum energy (P > 100 and E > 2.0) and speed and density of solar wind particles were selected as test parameters for the further research.

5 Parallel calculations for finding optimal models

For easy formalization of the models, we combine the output time series into a target vector and the input parameters into

a vector of parameters:

$$T = (T_1, T_2, T_3, T_4, T_5, T_6), \tag{2}$$

$$X = (X_1, X_2, X_3, X_4, X_5), \tag{3}$$

where T_i is the time series of the wind speed and pressure of Irma, Jose, and Katia hurricanes, respectively; X_j is the time series of P > 100, E > 2.0, speed of solar wind particles, density of solar wind particles, and F10.7, respectively.

The task is to find for each T_i the most accurate and adequate functional dependence of the type:

$$T_i = F_i(X, L_i, \Omega_i), \tag{4}$$

where $L_i = \{l_{ij}\}_{j=1,5}$ is the vector of optimal lags and Ω_i is a parameter of the linear or the artificial neural network model.

The determination coefficient (R^2) and mean square error (MSE) were considered as criteria of optimization. As further calculations have shown, in most cases the model with the maximum determination coefficient and the minimum mean square error coincided. In the case of differences in these models, models with the maximum value of the determination coefficient were more adequate. Therefore, further research usesed the determination coefficient as a criterion of adequacy.

Cross-validation (*cv*) for *k*-blocks (*k*-fold) was used to verify the accuracy of the models (Trippa et al. 2015). The training sample was divided into k blocks of the same size. Each block alternately was as a test sample, and the other $k-1$ blocks were a training sample. The goal function of optimization model was to maximize the determination coefficient R_i^2 between target vector T_i and the cross-validation results of model $F_i^{cv}(X, L_i, \Omega_i)$. Test calculations show that the best accuracy was obtained where the size of the test sample was 10% of the total size of the training sample, i.e. $k = 10$. In general, the optimization problem has the form:

$$R_i^2(T_i, F_i^{cv}(X, L_i, \Omega_i)) \xrightarrow{yields} \max \tag{5}$$

Solution variables: $L_i \in Ts,\ \Omega_i$

Limitations:

$$\{l_{ij}\}_{j=\overline{1-5}} \le Lag_{\max},$$

where Ω_i is the parameters of the model, which are determined by fitting the initial model data to the target vector, the fitting method depends on the type of model (linear, neural network, etc.). Ts – set of vector L_i lag combinations.

The optimization was done by completely scanning all possible combinations of the lag vector L_i for each component of vector X from 0 to 22 ($Lag_{\max} = 22$). The magnitude of the maximum lag was chosen from the preliminary analysis of Table 4, where the maximum lag was 20. Therefore, it was decided to check two lags more. The total number of all possible combinations of lags consists of $23^5 = 6{,}436{,}343$. Where 5 – numbers of vector X components. The all possible lag combinations Ts is defined as a set of tuples:

$$Ts(22) = \left\{\left\langle ts_1^{t1}, ts_2^{t2}, ts_3^{t3}, ts_4^{t4}, ts_5^{t5}\right\rangle\right\}_{t1,t2,t3,t4,t5=\overline{0-22}}, \tag{6}$$

where ts_j^{tj} – the value of lag for components of L_i vector.

For cross-validation, it is necessary to optimize each model 10 times plus one additional for a full set of values of the training sample. Such optimization should be performed for each element of the target vector, which is six. With this in mind, the total number of models that need to be optimized will be: $23^5 \cdot 11 \cdot 6 = 424{,}798{,}638$. Such a huge number of tasks requires an optimal choice for both the type of model (see Eq. (4)) and optimization algorithms.

In order to reduce the number of tested lags, an algorithm for finding an optimal model was proposed:

1. The first maximum number of lags is determined by $lag = 0$.
2. A set of tasks is formed based on Eq. (6).
3. For the first run *Tasks* (*lag*).
4. For next runs in order to avoid repetitions of tasks the difference of sets needs to be calculated $Tasks(lag)' = Tasks(lag) \backslash Tasks(lag\text{-}1)$.
5. The optimal model is found according to Eq. (5).
6. If the maximum lag value for any component of the optimal model does not exceed *lag-2*, it is assumed that the optimal value is found and the algorithm is completed.
7. If $lag = 22$, the algorithm is completed and is considered to have no optimal value.
8. Increase $lag+ = 1$ and move to step 1.

The presence of the set of several independent tasks which use the same memory area makes it possible to use parallel calculations by forming a pool for multiprocessing tasks, according to Eq. (5). The task with a specific tuple of lags was alternately selected from the pool and sent to the free core of the processor "worker" for calculation. After calculating all tasks, a function with a maximum determination coefficient was found and the conditions 4 and 5 of the algorithm were checked (Palach 2014).

Linear models were selected as test cases. Combination of the proposed algorithm and parallel calculation allowed us to reduce calculation time, about 10 times, and determination of optimal lags for each of the input parameters for all goal vectors.

6 Refinement of models using artificial neural networks

As a result of the preliminary analysis, six linear models are obtained using Eq. (4). That is why the parameters of linear

models Ω_i T and the lags of input parameters L_i are known. The identified lags were the basis for refinement of models with the artificial neural networks. As can be seen from Table 1, the maximum size of the training samples is 66, and a minimum is 15 records. Each neural network must have an input layer comprised of five neurons. Such a small size of the training sample puts some restrictions on the size of neural networks and the possibility of their adequate training. Multilayer perceptrons (MLPs) with back propagation were chosen (Géron 2017). The method of training was as a quasi-Newtonian method of optimization. A logistic function was selected as an activation function.

As test calculations have shown, the best results were observed for single-layered neural networks with the number of neurons in a hidden layer, which equals seven. Decreasing the number of neurons in the hidden layer reduced the network's ability to learn. Increasing the number of neurons in the hidden layer, on the contrary, led to retraining. Namely, on the one hand, the results of learning on the training set have improved significantly, but on the other side, significant fluctuations in the results of the cross-validation test appeared. However, even in the best of cases, there were from one to two abnormal fluctuations in the results of models, which disappeared during repeated training in one place of the time series and appeared in another. To remove these fluctuations, Delphi expert valuation method was used (Chang et al. 2000). Its essence was:

1. Several neural networks were created and studied for each model according to Eq. (4). In our case, their optimal number was nine. Their increase did not improve the result.
2. Predictive values were calculated on the test sets of data using the cross-validation method for each of the networks. The result was a matrix of type:

$$Res_i = \begin{bmatrix} f_{i1}^1 & \cdots & f_{im}^1 \\ \vdots & \ddots & \vdots \\ f_{i1}^9 & \cdots & f_{im}^9 \end{bmatrix}, \tag{7}$$

where m is the size of the training sample for a particular vector of the goals, the upper index is the serial number of the neural network.

3. Each column was sorted and then 10% of records with minimum and maximum values were removed from the records.
4. For the remaining values for each of the columns, the median was determined, which was considered to be the result.

As a result of this phase, unlike linear models, for each of the target vectors a list of nine trained neural networks was received: $T_i = \{F_i^n(X, L_i, \ \Omega_{i,n}^{ANN})\}_{n=\overline{1-9}}$. The total number of neural networks was: $6 \cdot 9 \cdot 11 = 594$, considering that for each cross-validation, 10 neural networks +1 network were constructed and studied on the complete training sample (necessary for further sensitivity analysis). To reduce the computer time, parallel calculations were also used (the same as at the cross-validation level).

7 Forecasting using recurrent neural networks

One of the disadvantages of the above-mentioned approaches is that they do not take into account the cumulative effect of the input field's behavior during the studied lag. That is, they take into account only one value of the input factors shifted to a certain time interval. However, a situation may arise where the behavior of only one factor over a certain period can lead to a crisis event. As noted above, linear models and back propagation neural networks cannot be used for this, as the number of input parameters will significantly increase. The solution to this situation is the use of recurrent neural networks (Greff et al. 2017). Feedback connections are implemented in which the output signal is fed to the input layer as additional inputs in order to take into account the time behavior of the fields in the system. Thus, the output signal depends on the previous state of the system. Iteratively scrolling the signal, you can consider the behavior of the system for a certain number of lagging steps.

In addition to this, it should be kept in mind that source factors depend not only on the above-mentioned 5 input factors. This is a complex nonlinear system, which depends on many factors not considered in the task. It is necessary to add as input factors the value of the output factor at previous moments to take into account their complex effect. To accomplish this the data set must be transformed into a three-dimensional form in the following way:

$$\begin{aligned} X_L^i = \big(&X_1(t-1), \ldots, X_5(t-1), T_i(t-1), \\ &X_1(t-t_L), \ldots, X_5(t-t_L), T_i(t-t_L) > \big) \end{aligned} \tag{8}$$

$$\begin{aligned} X_{3D,L}^i = \Big(&X_1(t-l)_{l=\overline{1,L}}, \ldots, X_5(t-l)_{l=\overline{1,L}}, \\ &T_i(t-l)_{l=\overline{1,L}}\Big) \end{aligned} \tag{9}$$

where t is row index, L is maximum lag value, and i is target index (2).

Output fields remain unchanged. Thus, we can see that the number of input fields has increased by 1 due to adding the output field. Each input represents an array of field values for a previous time lag L. Such a transformation of the data set allows us to eliminate the dimensional problems and take into account the behavior of input parameters over the previous period. On the other hand, it is necessary to take into account the previous values of the target factor. This

means that the number of rows in the data set will be reduced by the number of studied lags L. This, with a limited size of data set, significantly reduces the size of the investigated lag L. That is why that it is impossible to take into account lag = 22 for LSTM recurrent Neural networks in this case. The time interval $L = 4$ hours was chosen for investigation.

A recurrent neural network with long short-term memory (LSTM) was selected as an investigation model. This neural network allows you to simulate the behavior of a system that depends on time delay. This is realized by reverse transmission of the neural network output signal at the time $t - 1$ back to the input of one of the network layers. This complex input is used to calculate the output for time t.

LSTM is a type of the recurrent neural network, that allows memorizing values for long or short periods. This network does not use activation functions within its recurrent components. Thus, the stored value does not disappear iteratively over time.

The LSTM blocks contain three or four "valves" that they use to control the information flow to or from their memory. These valves are used as logistic function to calculate values between 0 and 1. This value multiplies the allowance or denial a partial flow of information to or from that memory (Greff et al. 2017).

LSTM represents themselves a neural network that is why the final value was calculated analogously to the classical neural network by the Delphi method.

8 Parallel calculations results of artificial neural networks and linear models

The best way to describe how modeled data fit the real data is to plot them on the single graph for each hurricane that has been the subject of this study. The results of calculations for linear models and artificial neural networks are presented in Fig. 4.

As can be seen from Fig. 4, in the majority of cases, LSTM models show the best prediction result for all six target vectors under study. Assigned before, only 4 hours lag was used in calculations in LSTM RNN. This means that the behavior of input factors at previous moments plays a key role in hurricane forecasting. The results for artificial neural networks and linear models are similar for the Irma and Jose hurricanes (i.e. wind speed). As can be seen from Figs. 4d–4f neural networks show significantly worse results than LSTM and linear models. In the case of the Katia hurricane, the lag of the optimal model for the RadioFlux field, which is four and zero, is also strange. This is completely inconsistent with the previous analysis. This can be explained by the small dataset size (15 records) and, accordingly, the inability of adequate training for both linear and neural networks. Regarding the Irma and Jose hurricanes, the obtained lags are in good agreement with the previous analysis for the RadioFlux field, which is the most influential (as it has been shown above). A quantitative comparison of the accuracy of results is presented in Table 5.

As can be seen from the table, the biggest determination coefficient is observed for the LSTM models in all predictions. The cross-validation testing confirmed that these models are accurate and adequate in the event of the hurricane Irma. The small cross-validation coefficient for Jose can be explained by the small lags that were taken into account in LSTM models. The bad results for the Katia test can be explained by too small data set that lead to overfitting of the LSTM model. In booth case (Irma and Katia) we need to use more data to use LSTM models. That is mean that these models are not adequate for this booth hurricanes.

Table 5 shows that the highest determination coefficients are obtained for target vectors such as the wind speed of the Irma hurricane, the pressure of the Irma hurricane, and wind speed of the Jose hurricane. Determination coefficients for linear models and neural networks coincide. Cross-validation results are slightly lower, but they also have high values. This also confirms the adequacy of these models. The table also demonstrates that pressure of the Jose hurricane has low values of determination coefficients for both the linear models and for neural networks. Therefore, the accuracy of this model is low. Regarding the Katia hurricane, it should be noted that similarly to the graphs, the results are accurate for linear models and low for neural networks, which may be caused by the small amount of the training sample and overfitting on models.

During the calculations, the following optimal linear models were obtained:

$$F_1\left(X, L_1, \Omega_1^{Lin}\right) = -16.44 - 1.09 \cdot x(3)_1 + 2.88 \cdot 10^{-04} \cdot x(13)_2 - 0.05 \cdot x(11)_3 + 0.85 \cdot x(2)_4 + 1.40 \cdot x(7)_5, \quad (10)$$

$$F_2\left(X, L_2, \Omega_2^{Lin}\right) = 1067.52 + 0.55 \cdot x(2)_1 - 5.42 \cdot 10^{-04} \cdot x(2)_2 + 0.02 \cdot x(12)_3 + 0.63 \cdot x(11)_4 - 1.17 \cdot x(10)_5, \quad (11)$$

$$F_3\left(X, L_3, \Omega_3^{Lin}\right) = -80.15 - 0.71 \cdot x(4)_1 + 4.93 \cdot 10^{-04} \cdot x(19)_2 + 0.12 \cdot x(3)_3 + 1.62 \cdot x(14)_4 + 0.84 \cdot x(18)_5, \quad (12)$$

$$F_4\left(X, L_2, \Omega_2^{Lin}\right) = 1073.42 + 0.54 \cdot x(5)_1 - 2.83 \cdot 10^{-04} \cdot x(2)_2 - 0.08 \cdot x(4)_3 - 1.27 \cdot x(11)_4 - 0.52 \cdot x(19)_5, \quad (13)$$

$$F_5\left(X, L_5, \Omega_5^{Lin}\right) = -413.61 - 94.62 \cdot x(2)_1 - 8.08 \cdot 10^{-04} \cdot x(6)_2$$

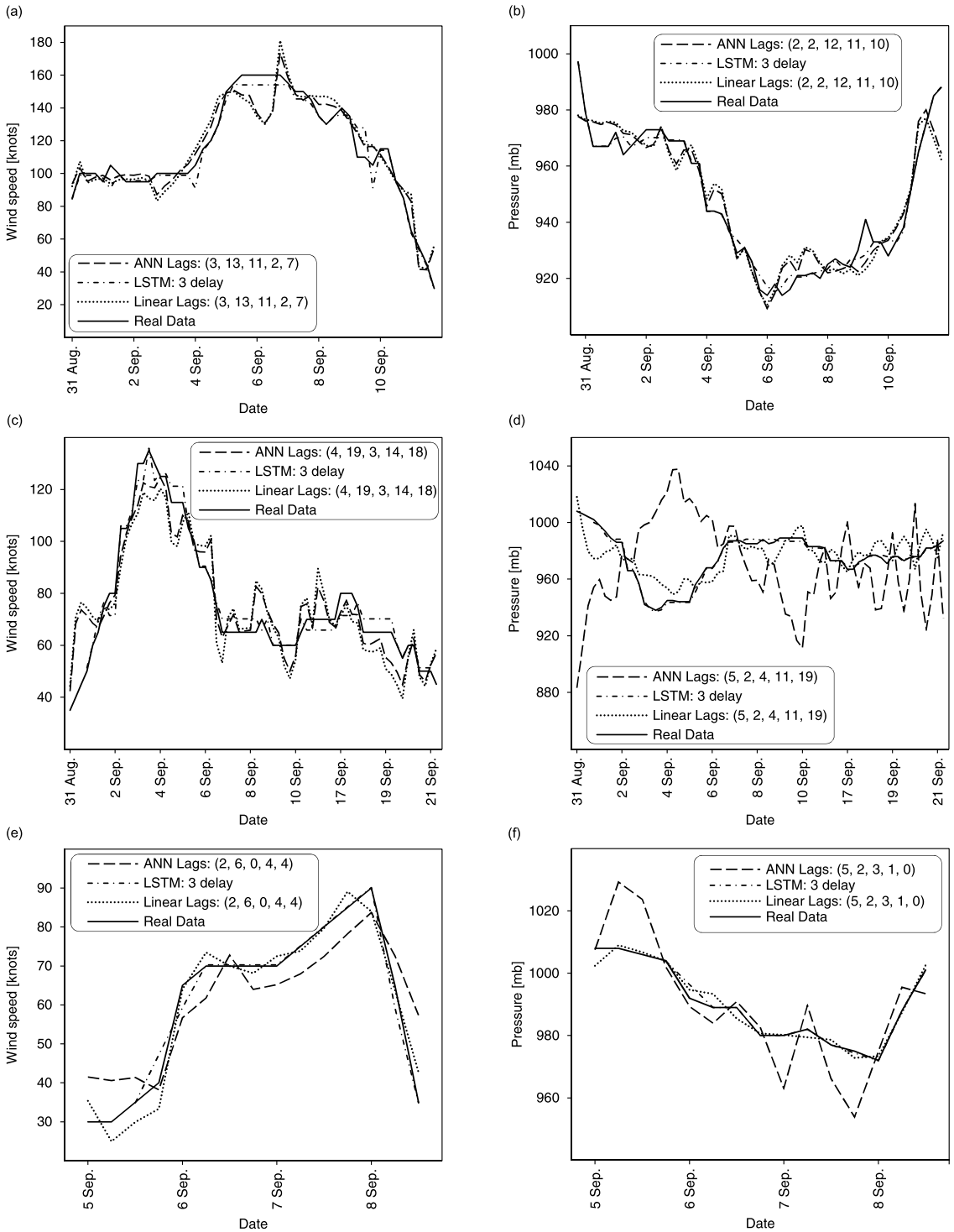

Fig. 4 Results of hurricane forecasting with linear models and artificial neural networks for: (a) Wind speed of the Irma hurricane, (b) Pressure of the Irma hurricane, (c) Wind speed of the Jose hurricane, (d) Pressure of the Jose hurricane, (e) Wind speed of the Katia hurricane, (f) Pressure of the Katia hurricane

$$+0.17\cdot x(0)_3 - 1.88\cdot x(4)_4 + 3.14\cdot x(4)_5, \quad (14)$$

$$F_6\left(X, L_6, \Omega_6^{Lin}\right) = 783.42 - 26.24\cdot x(5)_1 + 1.42\cdot 10^{-04}\cdot x(2)_2 + 0.12\cdot x(3)_3 - 2.30\cdot x(1)_4 + 1.19\cdot x(0)_5, \quad (15)$$

Table 5 Lags and determination coefficients of obtained models

Hurricane	Parameter	Model		Numbers of tests models	Lags	R^2 Full dataset	R^2 Cross validation
		Equation	Type				
Irma	Wind speed	$F_1(X, L_1, \Omega_1^{Lin})$	Linear	1,048,576	$L_1 = (3, 13, 11, 2, 7)$	0.89	0.85
		$\{F_1(X, L_1, \Omega_1^{ANN})\}$	ANN	99		0.89	0.75
		$\{F_1(X_{3D,L}, L_{LSTM}, \Omega_1^{LSTM})\}$	LSTM	99	$L_{LSTM} = \{l_i = \overline{1,4}\}\_i = \overline{1,6}$	0.98	0.88
	Pressure	$F_2(X, L_2, \Omega_2^{Lin})$	Linear	759,375	$L_2 = (2, 2, 12, 11, 10)$	0.90	0.88
		$\{F_2(X, L_2, \Omega_2^{ANN})\}$	ANN	99		0.90	0.87
		$\{F_2(X_{3D,L}, L_{LSTM}, \Omega_1^{LSTM})\}$	LSTM	99	$L_{LSTM} = \{l_i = \overline{1,4}\}\_i = \overline{1,6}$	0.99	0.93
Jose	Wind speed	$F_3(X, L_4, \Omega_4^{Lin})$	Linear	5,153,632	$L_3 = (4, 19, 3, 14, 18)$	0.86	0.77
		$\{F_3(X, L_4, \Omega_4^{ANN})\}$	ANN	99		0.86	0.74
		$\{F_3(X_{3D,L}, L_{LSTM}, \Omega_1^{LSTM})\}$	LSTM	99	$L_{LSTM} = \{l_i = \overline{1,4}\}\_i = \overline{1,6}$	0.98	0.61
	Pressure	$F_4(X, L_4, \Omega_4^{Lin})$	Linear	5,153,632	$L_4 = (5, 2, 4, 11, 19)$	0.69	0.56
		$\{F_4(X, L_4, \Omega_4^{ANN})\}$	ANN	99		0.58	0.70
		$\{F_4(X_{3D,L}, L_{LSTM}, \Omega_1^{LSTM})\}$	LSTM	99	$L_{LSTM} = \{l_i = \overline{1,4}\}\_i = \overline{1,6}$	0.98	0.45
Katia	Wind speed	$F_5(X, L_5, \Omega_5^{Lin})$	Linear	100,000	$L_5 = (2, 6, 0, 4, 4)$	0.98	0.96
		$\{F_5(X, L_5, \Omega_5^{ANN})\}$	ANN	99		0.72	0.34
		$\{F_5(X_{3D,L}, L_{LSTM}, \Omega_1^{LSTM})\}$	LSTM	99	$L_{LSTM} = \{l_i = \overline{1,4}\}\_i = \overline{1,6}$	0.95	0.48
	Pressure	$F_6(X, L_6, \Omega_6^{Lin})$	Linear	59,049	$L_6 = (5, 2, 3, 1, 0)$	0.98	0.96
		$\{F_6(X, L_6, \Omega_6^{ANN})\}$	ANN	99		0.65	0.53
		$\{F_5(X_{3D,L}, L_{LSTM}, \Omega_1^{LSTM})\}$	LSTM	99	$L_{LSTM} = \{l_i = \overline{1,4}\}\_i = \overline{1,6}$	0.99	0.38
Total			Linear	12,274,264			
			ANN	594			
			LSTM	594			

where the value of the lag is specified in the brackets of the input parameters.

The result of the training neural networks is represented by 54 neural networks whose parameters change during the training, so it is not expedient to bring several dynamic matrices of neurons' weight factors.

The total number of tested linear models on account of the proposed algorithm using decreased from 424,798,638 to $12{,}274{,}264 \cdot 11 = 135{,}016{,}904$, i.e. the total number of models is reduced to 32% of the previous indicator.

The using of neural networks within such an algorithm takes several orders more time and requires, accordingly, the involvement of a computer cluster.

9 Sensitivity analyses

To verify the adequacy of the models an analysis of the model's sensitivity to the change of factors for all models in Table 5 was performed (Pianosi et al. 2016). The analysis was as follows. For each tuple r of the input parameters vector $X^r = \{x_j^r\}_{\substack{j=\overline{1-5} \\ r=\overline{1-N}}}$, (for LSTM models x_j^r is a vector of values during the lag L) which consists of N records, the input parameters value was incremented by 10% and the change of the corresponding model $F_{i=\overline{1-6}}$ or the set of models was calculated by the Delphi method (in the case of neural networks). Then all the obtained values were averaged. The resulting value represents the average change in wind speed or pressure of the particular hurricane with an increase of the input parameter by 10%.

To implement this, a diagonal matrix of variation factors was created with a dimension equal to the number of input parameters, in our case, five:

$$V = \begin{bmatrix} 0.1 & \cdots & 0 \\ \vdots & \ddots & \vdots \\ 0 & \cdots & 0.1 \end{bmatrix}_{5\times 5}. \tag{16}$$

Each tuple of the input parameters vector is duplicated vertically in the amount which equals the length of the tuple (that is, the number of input parameters):

$$A^r = \begin{bmatrix} x_1^r & \cdots & x_5^r \\ \vdots & \ddots & \vdots \\ x_1^r & \cdots & x_5^r \end{bmatrix}. \tag{17}$$

The matrix of test values was calculated as an elemental product of matrices:

$$T^r = (V+1)\cdot A^r = \begin{bmatrix} 1.1\cdot x_1^r & \cdots & 1.0\cdot x_5^r \\ \vdots & \ddots & \vdots \\ 1.0\cdot x_1^r & \cdots & 1.1\cdot x_5^r \end{bmatrix}. \quad (18)$$

The vector of values was calculated:

$$S_i^r = F_i\left(T^r, L_i, \Omega_i^{Lin(ANN)}\right) = \begin{bmatrix} f_{i,x_1}^r \\ \vdots \\ f_{i,x_5}^r \end{bmatrix}. \quad (19)$$

An array of obtained changes of functions F_i is formed by estimating the values S_i^r for all tuples of vector X:

$$S_i = \begin{bmatrix} (S_i^1)^T \\ \vdots \\ (S_i^N)^T \end{bmatrix}. \quad (20)$$

Then the vector values predicted by the model was calculated and duplicated horizontally by the amount of input fields:

$$M_i = \left\{m_i^r\right\}_{r=\overline{1-N}} = F_i\left(X, L_i, \Omega_i^{Lin(ANN)}\right), \quad (21)$$

$$Mx_i = \begin{bmatrix} m_i^1 & \cdots & m_i^1 \\ \vdots & \ddots & \vdots \\ m_i^N & \cdots & m_i^N \end{bmatrix}_{N\times 5}. \quad (22)$$

The last step was building a matrix of relative changes by calculating the elemental difference and dividing the matrices Mx_i and S_i. Then averaging by the columns is performed:

$$D = (S_i - Mx_i)/Mx_i, \quad (23)$$

$$Sens = \overline{D}_{col}. \quad (24)$$

The results of the calculations are given in Table 6.

As can be seen from the table, we got different results between the LSTM models and Linear with ANN. It can easily be explained by a different approach by taking into account the time lag behavior of input factors. Also, a different time lag was used for these models. Therefore sensitivity analysis should be done separately for these models.

As was shown before, the best models were obtained for the Irma hurricane by the LSTM models. The sensitivity analysis shows that the increasing Density during 4 hours by 10% will lead to increasing of the wind speed by 40%. Increasing of factors like P > 100, E > 2.0 and Speed will decrease the wind speed. Also, this calculation shows that Sun's activity weakly impacts on pressure.

The most sensitive factor for Jose is F10.7. Increasing this factor by 10% will lead to increasing speed by 123% and decreasing pressure by 45%. These big numbers can be explained by not good adequacy of the LSTM model for this hurricane. A similar situation is observed for the Katia hurricanes.

For the Linear and ANN models, as can be seen from Table 6, the factor that has the greatest impact on the wind speed of the hurricanes is F10.7. Its increase by 10% leads to an increase in the wind speed for the Irma hurricane on average by 13%–14% in 42 hours (lag 7) and 11% in 4.5 days (lag 18) for Jose. As the table shows, indicators of linear models and neural networks are sufficiently close for all factors and these hurricanes, which confirm the adequacy of the models. The second important indicator is the speed of SW. Its increase by 10% raises the hurricane Jose's speed by 9% after 18 hours (lag 3) and decreases the hurricane Irma's speed by 2.5% after 3 days. Other factors do not affect these two hurricanes.

For the Katia hurricane, the sensitivity of wind speed on F10.7 is 74% for the linear models and only 3% for neural networks. A strong difference in the sensitivity of neural network and linear models also calls into question their adequacy. This may be caused by a small amount of data, which prevented the construction of an adequate model.

As known, the root cause of the wind is the pressure drop, so it is interesting to analyze the influence of the SW parameters on air pressure. If we analyze the sensitivity of the pressure for the Irma and Jose hurricanes, we can see that they are less sensitive to changes in SW. In particular, changing the F10.7 by 10% causes a pressure drop of 1.3% after 2.5 days for the Irma hurricane and practically does not affect the pressure of the hurricane Jose. However, as can be seen from Fig. 2, the indicated parameter has increased from August 28 to September 4, 2017, from 82.4 to 140, that is, by 70%. According to Table 6, the change in only one of these factors had to cause a pressure change in the hurricane zone at $0.7/0.1(-1.3\%) = -9.5\%$, that is, from 1004 mb to 908 mb. The actual recorded pressure was 914 mb (forecast error is 0.6%). For the hurricane Jose, the calculated change is 971 mb, the recorded is 938 mb (forecast error is 3.5%). Thus, despite the low sensitivity of pressure on change of the parameters of SW, strong fluctuations of the input parameters can cause a sharp decrease in pressure, and hence the emergence of hurricanes.

10 Conclusions

Considering the potential prognostic models, one should certainly bear in mind that for solar flares from active regions located at the east heliolongitude, the time delay (between emission and the ground level enhancement onset) can be from several hours up to days. Almost all diffusion

Table 6 Sensitivity analysis of the obtained models

Hurricane	Parameter	Model	P > 100	E > 2.0	Speed	Density	F10.7
Irma	Wind speed	Linear	−0.63%	0.10%	−2.51%	0.23%	14.38%
		ANN	−0.65%	0.13%	−2.64%	0.18%	13.05%
		LSTM	−12.76%	−8.94%	−28.36%	40.35%	0.46%
	Pressure	Linear	0.02%	−0.04%	0.09%	0.02%	−1.36%
		ANN	0.02%	−0.04%	0.09%	0.02%	−1.36%
		LSTM	0.15%	−0.99%	−1.77%	−0.64%	0.20%
Jose	Wind speed	Linear	−0.26%	0.50%	9.27%	0.64%	11.27%
		ANN	−0.26%	0.50%	9.27%	0.64%	11.27%
		LSTM	−0.03%	−18.31%	1.89%	−4.21%	123.51%
	Pressure	Linear	0.01%	−0.04%	−0.42%	−0.04%	−0.53%
		ANN	0.00%	0.59%	3.63%	0.43%	5.24%
		LSTM	−0.02%	−0.43%	−6.93%	3.99%	−44.84%
Katia	Wind speed	Linear	−1.07%	−1.19%	17.69%	−1.17%	74.57%
		ANN	0.00%	−1.30%	8.80%	−0.64%	3.33%
		LSTM	4.77%	24.89%	547.95%	207.05%	0.80%
	Pressure	Linear	−0.02%	0.05%	0.66%	−0.07%	1.46%
		ANN	0.00%	−0.14%	2.65%	0.50%	6.98%
		LSTM	−3.33%	1.47%	7.15%	−9.92%	−8.46%

models involving solar particle transport in the interplanetary medium show that the maximum time delay is proportional to the square of the distance traveled (Augusto et al. 2013).

The efficiency of the penetration depends on the degree to which the interplanetary magnetic field provides input of the particle flux to the region with the given angle, and/or the percentage relation the particles of the given direction are present in the flux with high angular isotropy.

Two different approaches were tested to take into account the time delays between the parameters of solar activity and the main characteristics of the hurricanes in this research. In the first approach, a set of linear models with all possible lags of input parameters was investigated. The best of the models were refined using be artificial neural networks. The second approach was to use recurrent neural networks LSTM. The time series of SW was chosen as input parameters for the training and testing. This makes it possible to take into account the influence of the dynamics of changes in input parameters on the characteristics of hurricanes. The last approach has made it possible to describe and impart the best of hurricane dynamics.

Research in this paper has shown that the applied model is accurate and adequate to predict the appearance of hurricanes 2–4 days ahead, after the outbreak of SW. High determination coefficients sustain the previous conclusion. The model can explain about 90% of variations of the Irma hurricane. Jose is the hurricane in the Pacific Ocean, which has a larger scale, and therefore the processes of the influence of external factors are more inertial, which explains a bigger lag in the calculations. The sensitivity analysis revealed that F10.7 has the greatest impact on the hurricane wind speed, except for the case of the Katia hurricane. In the general picture of the change in pressure and wind speed over a longer period, the other factors were not taken into account in the model. Therefore, the model for Jose was less accurate but quite adequate. As already has been noted in Sect. 8, the Katia hurricane was the least lengthy and the data were not sufficient to test the hypothesis in this case. In all cases, LSTM models showed the best results. But for effective use, big data sets should be obtained.

Nikolić et al. (2010), at the same time, explained that charged particles can be associated with the origin of cyclonic airmass moving, which doesn't always have to be represented exclusively by the hurricanes. Radovanović et al. (2013) faced similar observations in the case of tornadoes in Serbia. Gomes et al. (2012), among other things, considered a physical mechanism, which could explain a possible connection. According to these authors, the appearance of hurricanes Katrina, Rita, and Wilma are directly dependent on the appropriate re-emergence of energy regions in the sun in geoeffective position.

We can assume that the above results Vyklyuk et al. (2017a), Vyklyuk et al. (2017b), and the results obtained in this study are connected with the nature of the data used by the ACE satellites. Namely, the position of this satellite is

always located between the sun and the earth and that in the relative time it measures the changes in the solar wind parameter that is directed towards the Earth. This means that after passing, for example, a particular energy region through a geo-effective position, the ACE satellite no longer detects the flow of high-energy particles. It is possible that this connection could not be registered because the interplanetary magnetic field is moving in the form of curved lines. Therefore, we consider that the continuation of the research should be directed towards obtaining and processing data on the parameters of the solar wind, which are directed to our planet, which can be measured by other satellites.

Acknowledgements All original data used in this paper are publicly available. The wind speed and the central pressure data of the Irma, Jose and Katia hurricanes were downloaded from the Unisys archive of hurricanes data. The Data Service Base of the Space Weather Prediction Center (SWPC) was the source of solar particles and electron flux data, while data on proton speed and proton density were obtained from data archive of the SOHO CELIAS Proton Monitor. This paper is a result of the project "Geografija Srbije" (No. III47007) funded by the Ministry of Education, Science and Technological Development of the Republic of Serbia.

References

Artamonova, I.V., Veretenenko, S.V.: Geomagn. Aeron. **53**, 5–9 (2013). https://doi.org/10.1134/S0016793213010039

Augusto, C.R.A., Kopenkin, V., Navia, C.E., Felicio, A.C.S., Freire, F., Pinto, A.C.S., Pimentel, B., Paulista, M., Vianna, J., Fauth, C., Sinzi, T.: (2013). arXiv:1301.7055

Bajčetić, J.B., Nina, A., Čadež, V.M., Todorović, B.M.: Therm. Sci. **19**(Suppl. 2), S299–S309 (2015). https://doi.org/10.2298/TSCI141223084B

Chang, P.T., Huang, L.C., Lin, H.J.: Fuzzy Sets Syst. **112**(3), 511–520 (2000). https://doi.org/10.1016/S0165-0114(98)00067-0

Cohen, J., Cohen, P., West, S.G., Aiken, L.S.: Applied Multiple Regression/Correlation Analysis for the Behavioral Sciences, 3rd edn. Routledge Taylor & Francis Group, New York, Oxford (2013)

Elsner, J.B., Kavlakov, S.P.: Atmos. Sci. Lett. **2**(1–4), 86–93 (2001). https://doi.org/10.1006/asle.2001.0043

Elsner, J., Jagger, T., Dickinson, M., Rowe, D.: J. Climate **21**(6), 1209–1219 (2008). https://doi.org/10.1175/2007JCLI1731.1

Frank, M.W., Young, S.G.: Mon. Weather Rev. **135**(10), 3587–3598 (2007). https://doi.org/10.1175/MWR3435.1

Fritsch, F.N., Carlson, R.E.: SIAM J. Numer. Anal. **17**(2), 238–246 (1980). https://doi.org/10.1137/0717021

Géron, A.: Hands-on Machine Learning with Scikit-Learn and TensorFlow: Concepts, Tools, and Techniques to Build Intelligent Systems. O'Reilly Media, Inc., Sebastopol (2017).

Gomes, J.F.P., Mukherjee, S., Radovanović, M.M., Milovanović, B., Popović, C.L., Kovačević, A.: In: Escaropa Borrega, C.D., Beirós Cruz, A.F. (eds.) Solar Wind: Emission, Technologies and Impacts, pp. 1–46. Nova Science Publishers, Hauppauge, New York (2012)

Greff, K., Srivastava, R.K., Koutník, J., Steunebrink, B.R., Schmidhuber, J.: IEEE Trans. Neural Netw. Learn. Syst. **28**(10), 2222–2232 (2017). https://doi.org/10.1109/TNNLS.2016.2582924

Haigh, J.D.: Science **272**(5264), 981–984 (1996). https://doi.org/10.1126/science.272.5264.981

Hodges, R., Elsner, J.: ISRN Meteorol. **2012**, 517962 (2012). https://doi.org/10.5402/2012/517962

Hodges, R.E., Jagger, T.H., Elsner, J.B.: Nat. Hazards **73**(2), 1063–1084 (2014). https://doi.org/10.1007/s11069-014-1120-9

Japan Aerospace Exploration Agency Earth Observation Research Center: Tropical cyclones track 2017 season. http://sharaku.eorc.jaxa.jp/cgi-bin/typ_db/typ_track.cgi?lang=e&area=AT. Cited 10 Jan 2018 (2017)

Mendoza, B., Pazos, M.: J. Atmos. Sol.-Terr. Phys. **71**(17–18), 2047–2054 (2009). https://doi.org/10.1016/j.jastp.2009.09.012

Mihajlović, J.: J. Geogr. Inst. Cvijic. **67**(2), 115–133 (2017). https://doi.org/10.2298/IJGI1702115M

Morozova, A.L., Pudovkin, M.I., Thejll, P.: Int. J. Geomagn. Aeron. **3**(2), 181–189 (2002)

Mukherjee, S.: Extraterrestrial Influence on Climate Change. Springer, India (2013)

Mukherjee, S.: J. Earth Sci. Clim. Change **6**, 261 (2015). https://doi.org/10.4172/2157-7617.1000261

Nikolić, L.J., Radovanović, M.M., Milijašević, P.D.: Nucl. Technol. Radiat. Protect. **25**(3), 171–178 (2010). https://doi.org/10.2298/NTRP1003171N

Olden, J.D., Neff, B.D.: Mar. Biol. **138**(5), 1063–1070 (2001). https://doi.org/10.1007/s002270000517

Palach, J.: Parallel Programming with Python. Packt Publishing Ltd., Birmingham (2014)

Pianosi, F., Beven, K., Freer, J., Hall, J.W., Rougier, J., Stephenson, D.B., Wagener, T.: Environ. Model. Softw. **79**, 214–232 (2016). https://doi.org/10.1016/j.envsoft.2016.02.008

Prikryl, P., Rusin, V., Rybanský, M.: Ann. Geophys. **27**, 1–30 (2009a). https://doi.org/10.5194/angeo-27-1-2009

Prikryl, P., Muldrew, D.B., Sofko, G.J.: Ann. Geophys. **27**, 31–57 (2009b). https://doi.org/10.5194/angeo-27-31-2009

Prikryl, P., Iwao, K., Muldrew, D., Rusin, V., Rybansky, M., Bruntz, R.: J. Atmos. Sol.-Terr. Phys. **149**, 219–231 (2016). https://doi.org/10.1016/j.jastp.2016.04.002

Prikryl, P., Bruntz, R., Tsukijihara, T., Iwao, K., Muldrew, D.B., Rušin, V., Rybanský, M., Turňa, M., Šťastný, P.: J. Atmos. Sol.-Terr. Phys. (2017). https://doi.org/10.1016/j.jastp.2017.07.023

Radovanović, M.M.: J. Geograph. Instit. "Jovan Cvijic" SASA. **68**(1), 149–155 (2018). https://doi.org/10.2298/IJGI1801149R

Radovanović, M.M., Milovanović, B., Pavlović, A.M., Radivojević, R.A., Stevančević, T.M.: Nucl. Technol. Radiat. Protect. **28**, 52–59 (2013). https://doi.org/10.2298/NTRP1301052R

SOHO CELIAS Proton Monitor: MTOF/PM Data by Carrington Rotation. http://umtof.umd.edu/pm/crn/. Cited 2 Oct. 2017 (2017)

SolarMonitor.org, AIA 193Å 20170827 19:27. https://solarmonitor.org/full_disk.php?date=20170827&type=saia_00193&region. Cited 10 Jan 2018 (2017)

Space Weather Prediction Center: ftp://ftp.swpc.noaa.gov/pub/lists/particle/. Cited 2 Oct. 2017 (2017a)

Space Weather Prediction Center: ftp://ftp.swpc.noaa.gov/pub/indices/old_indices/2017Q3_DSD.txt. Cited 2 Oct. 2017 (2017b)

Todorović Drakul, M., Čadež, V.M., Bajčetić, J., Popović, L.Č., Blagojević, D., Nina, A.: Serb. Astron. J. **193**, 11–18 (2016). https://doi.org/10.2298/SAJ160404006T

Trippa, L., Waldron, L., Huttenhower, C., Parmigiani, G.: Ann. Appl. Stat. **9**(1), 402–428 (2015). https://doi.org/10.1214/14-AOAS798

Unisys: http://weather.unisys.com/hurricane/atlantic/2017/index.php. Cited 2 Oct. 2017 (2017)

Veretenenko, S.V.: Geomagn. Aeron. **81**(2), 281–284 (2017). https://doi.org/10.3103/S1062873817020460

Veretenenko, S., Thejll, P.: J. Atmos. Sol.-Terr. Phys. **66**(5), 393–405 (2004). https://doi.org/10.1016/j.jastp.2003.11.005

Vyklyuk, Y., Radovanović, M., Milovanović, B., Leko, T., Milenković, M., Milošević, Z., Milanović Pešić, A., Jakovljević, D.: Nat. Hazards **85**, 1043–1062 (2017a). https://doi.org/10.1007/s11069-016-2620-6

Vyklyuk, Y., Radovanović, M.M., Stanojević, G.B., Milovanović, B., Leko, T., Milenković, M., Petrović, M., Yamashkin, A.A., Milanović Pešić, A., Jakovljević, D., Malinović Milićević, S.: J. Atmos. Sol.-Terr. Phys. **180**, 159–164 (2017b). https://doi.org/10.1016/j.jastp.2017.09.008

Wheeler, D.: J. Atmos. Sol.-Terr. Phys. **63**(1), 29–34 (2001). https://doi.org/10.1016/S1364-6826(00)00155-3